

Genomics of rafting crustaceans reveals adaptation to climate change in tropical oceans

Received: 27 November 2024

Accepted: 27 January 2026

Published online: 06 February 2026

 Check for updates

Hongguang Liu^{1,2}, Jonathan M. Waters³, Mengyi Huang^{1,4}, Ziyang Wang^{1,4}, Wan-Jin Chang⁵, Shuqiang Li⁶ & Zhonghe Hou^{1,2} ✉

Rafting dispersal has been proposed as a way for coastal species to track climate-driven niche shifts. However, little information exists on how rafting species disperse and adapt to shifting environmental conditions, particularly ocean currents and salinity. Here, we integrate dispersal simulations, ecological genomics, and salinity stress experiments to investigate rafting dynamics and adaptive shifts in widely distributed crustaceans across the Indo-Australian Archipelago. We develop a quantified model to examine asymmetric gene flow between populations driven by recent seasonal oceanographic shifts. Our climatic and dispersal models suggest that rafting populations must cope with increasing salinity fluctuation caused by rapidly-shifting oceanic connectivity patterns. Our genomic data provide evidence for recent selective sweeps at osmoregulatory loci, and key duplications at glycoside hydrolase gene families. Our experimental data reveal plastic expression of osmoregulatory genes required for survival during long-distance rafting voyages. These synergies between rafting dispersal and genomic change highlight the potential for rafting species to adapt to rapidly shifting oceanographic conditions.

Rafting dispersal is thought to play a fundamental role in determining distributions of diverse marine and coastal organisms, and can facilitate direct responses to ecological disturbance and environmental change^{1–3}. Such long-distance voyages involve fluctuating climatic and oceanographic conditions and can potentially promote both biogeographic and adaptive shifts in rafting taxa^{4,5}. However, opportunities to understand rafting dispersal and its role in climate-driven biological shifts have been scarce, because such oceanographic events and associated genomic shifts remain challenging to directly observe and quantify⁶.

For species hitchhiking on rafting substrates, ocean currents can act as vehicles for directional dispersal, potentially leading to asymmetric gene flow and source-sink biodiversity patterns^{7–10}. Quantifying

such dispersal dynamics is crucial for understanding how oceanographic processes can influence the directionality and magnitude of gene flow. In many cases, long-distance rafting species must cope with thermal and salinity shifts occurring during voyages, and obtain energy from rafting substrates for months^{4,5}. In addition, under global change, shifting oceanographic conditions (accelerating currents; fluctuating salinity) present additional physical and metabolic challenges^{11–14}. Thus, there is an urgent need to address how rafting species disperse, adapt, and respond to shifting climates. Here, we address these questions by integrating oceanographic, physiological, and ecological genomic analyses.

Intertidal talitrid amphipods, which are broadly distributed in the tropical Indo-Australian Archipelago (IAA), are sensitive to

¹State Key Laboratory of Animal Biodiversity Conservation and Integrated Pest Management, Institute of Zoology, Chinese Academy of Sciences, Beijing, China. ²College of Life Sciences, Capital Normal University, Beijing, China. ³University of Otago, Department of Zoology, Dunedin, New Zealand. ⁴University of Chinese Academy of Sciences, Beijing, China. ⁵Xiamen University Malaysia, Jalan Sunsuria, Bandar Sunsuria, Sepang, Selangor, Malaysia. ⁶College of Life Sciences, Anhui Normal University, Wuhu, Anhui, China. ✉e-mail: houze@ioz.ac.cn

oceanographic change because they lack autonomous larval dispersal capacity and instead disperse primarily as adults with driftwood¹⁵. These taxa have been inferred to disperse passively via ocean currents for several thousands of kilometers^{1,16}, and during such journeys must cope with drastic salinity shifts (15 to 34 ppt). In addition, ocean currents in the IAA connecting the South China Sea and Indonesian waters show seasonal variation, shifting northward in summer and southward in winter^{17,18}, which have potential to impact gene flow between populations^{19,20}. Therefore, wide-distributed intertidal talitrids in this region present a strong system for assessing adaptive shifts in response to rapid environmental change.

In this study, we examine 203 talitrid samples across the IAA and sequence the genome of the widely distributed talitrid *Talorchestia martensii*. We also resequence the whole genome of 104 individuals to infer their population structure and demographic histories. Then, we integrate gene flow patterns and genetic simulation models to infer their potential dispersal patterns between different geographical regions. We develop and apply oceanographic models to further test the role of ocean currents in rafting dispersal. In addition, we incorporate genomic variants into environmental modeling to assess the relative maladaptation of different populations and predict dispersal dynamics under future oceanographic forecasts. To assess genetic responses to rafting dispersal, we experimentally quantify genomic and transcriptomic shifts linked to altered salinity and identify the duplication events of genes involved in wood-feeding. Overall, our results provide a model system for elucidating rafting dispersal driven by ocean currents and shed light on the genetic adaptation mechanisms that can underpin rafting dispersal.

Results

Population dynamics of intertidal crustaceans in Indo-Australian Archipelago

A total of 203 talitrid samples from 80 localities were examined, encompassing a substantial portion of the IAA coastline (Fig. 1a, Supplementary Fig. 1a and Supplementary Data 1). Based on the monophyletic relationship and *COI* distance threshold delimitation (16%)²¹, we identified *T. martensii* as the most abundant and widely distributed species (154 samples; Supplementary Fig. 1b, c). We first assembled a 647.1-Mb contig-level *T. martensii* genome and resequenced whole genomes from 104 samples to a mean genome-wide depth of coverage of $15 \times$ (range: 10.2–47.8 \times) per sample (Supplementary Table 1). Single-nucleotide polymorphism (SNP) calling and stringent quality filtering revealed 6,690,030 whole-genome SNPs. Based on retained SNPs after stringent quality-filtering, phylogenetic analysis, ADMIXTURE analyses ($K=5$), and principal component analysis (PCA) revealed five geographical populations: Vietnam-Thailand (VT), North Borneo (NB), East Borneo (EB), South Borneo (SB), and South Sulawesi (SS) (Fig. 1b, c, and Supplementary Fig. 2).

Divergence times and long-term effective population sizes for *T. martensii* were estimated by Pairwise Sequentially Markovian Coalescent (PSMC) method²² and G-PhoCS²³ using SNP data (Supplementary Figs. 3 and 4 and Supplementary Table 2). Our results suggest *T. martensii* originated ca. 2.5 million years ago (Ma) with a large effective population size (N_e), and then split into two major clades with smaller N_e (Fig. 1d and Supplementary Fig. 4a). One of these clades is distributed around South Sulawesi and East Borneo, and the other in Vietnam-Thailand, South Borneo, and North Borneo.

Genetic simulations indicate asymmetric northward gene flow

D-statistics revealed substantial gene flow between South Sulawesi and Vietnam-Thailand populations (Supplementary Table 3). The G-PhoCS²³ and TreeMix²⁴ indicated that northward gene flow (SS to VT) was stronger than southward gene flow (VT to SS) (Mann-Whitney U test, $P=0.024$; Fig. 1e, f). To further infer detailed population migration and gene flow patterns, we performed genetic simulations twice

using Fastsimcoal 2.7²⁵ with 25 simulation models in five populations ($K=5$), or 20 simulation models in three populations ($K=3$) (Supplementary Figs. 5 and 6 and Supplementary Table 4). Both simulations suggest asymmetric gene flow, with a northward dispersal model favored over random and southward dispersal models (Fig. 1g–i). The best northward model suggested that talitrids dispersed from the southern region (East Borneo and South Sulawesi) to the northern region (Vietnam-Thailand) through the central region (South Borneo and North Borneo) in a stepping-stone manner. In addition, a Mantel test performed on the pairwise geographical and genetic distances rejected isolation by geographical distance (Spearman's P -value = 0.5, Fig. 1g).

Quantified model suggests association of summer ocean currents with northward rafting

To test relationships between gene flow and ocean currents, we developed a novel model to quantify ocean currents between two sites based on the least-cost dispersal path (Fig. 2a). The direction and velocity of ocean currents play important roles in explaining gene flow between populations²⁶. We defined direction deviation (ΔD) as the angle between the direction of ocean currents and the least-cost path line. The ΔD was calculated as the average of each grid cell along the least-cost path line, and the larger value represents the mismatch between directions of ocean currents and potential dispersal direction. The dispersal velocity (V_{ds}) was the average value of the grid's effective dispersal velocity, which was calculated as the projection of the ocean current velocity (V_{oc}) onto the direction of the path. The transit time between sites was estimated by dividing the least-cost distance by dispersal velocity (Fig. 2a).

We tested the relationship between these quantified parameters and gene flow by correlation tests based on the following assumptions: (1) concordant dispersal direction with ocean currents (smaller ΔD) will contribute to higher gene flow; (2) faster dispersal velocity will contribute to higher gene flow, showing a positive relationship between velocity and gene flow; and (3) reduced transit time between two sites will contribute to higher gene flow (Fig. 2a).

As seasonal monsoons in IAA shift ocean current direction (northward flow from April to September, southward flow from October to March), correlation tests were conducted between gene flow and ocean current dynamics for each month from 2014–2016. The results suggest an opposite correlation between gene flow and ocean currents in winter and summer (Fig. 2b), in detail, gene flow was significant negative related to ocean current directions ($P=0.02$) and positive to ocean current velocity ($P=0.03$) in June (Fig. 2b, c). Due to the difference between the least-cost path and actual dispersal path, we simultaneously calculated transit times under two scenarios using equations in Fig. 2a and Lagrangian particle trajectory model²⁷ (Fig. 2d, e), and tested the correlation between transit time and gene flow. Both analyses yielded negative correlations (Fig. 2c and Supplementary Fig. 7).

To visualize the role of ocean currents in species dispersal and distribution, we simulated the raft trajectories of *T. martensii* by an individual-based Lagrangian particle trajectory model, with two drift simulations over eight months, one starting in April (summer drift) and the other in October (winter drift) (Supplementary Figs. 8 and 9). According to the results from models that integrated ocean currents and environmental temperature and salinity, intraspecific connectivity occurred with both winter and summer simulations. Nonetheless, the summer drift simulations (Fig. 2d) corresponded more closely to the contemporary distribution of *T. martensii* than did the winter simulations (Fig. 2e). For example, 14.6% of particles from SS reached VT in summer simulations, whereas only 0.7% reached SS from VT in winter simulations (Supplementary Table 5).

To investigate the effects of driftwood mass and shape, we varied the value of “wind_drift_factor” in OpenDrift²⁸. The results indicate that very large pieces of driftwood are likely to become stranded near their

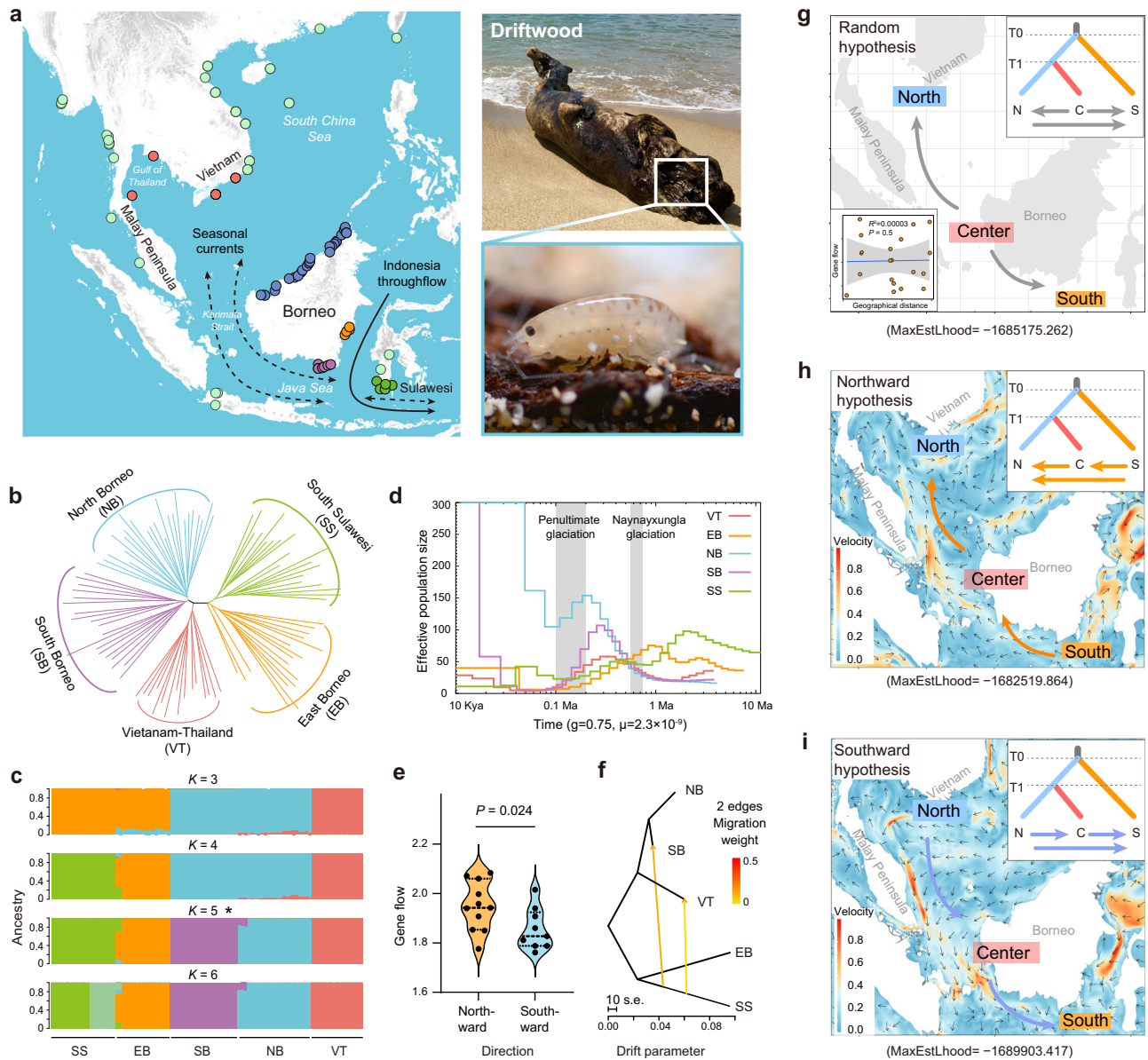


Fig. 1 | *Talorchestia martensii* sampling locations, population dynamics, and dispersal simulation models. **a** Collection sites included in this study. Colored dots correspond to *T. martensii* populations: Vietnam-Thailand (VT, red), North Borneo (NB, blue), South Borneo (SB, purple), East Borneo (EB, orange), and South Sulawesi (SS, green). Light green dots correspond to other talitrid species. The right pictures show driftwood in the coastal area and *T. martensii* on wood. **b** Unrooted phylogeny reconstructed using RAxML. **c** Population structure analysis of *T. martensii* from $K = 3-6$, in which $K = 5$ was the best-fit model. **d** Effective population size fluctuations of the five geographical populations estimated by PSMC. **e** Gene flow between populations estimated by G-PhoCS suggest northward gene flow ($n = 11$) is significantly greater than the southward ($n = 9$). Statistical significance was assessed using the two-tailed Mann-Whitney U test. **f** Two migration events estimated by TreeMix; arrows indicate northward migration, and are colored according to the

migration weight. **g-i** Alternative hypotheses of dispersal and genetic simulations. The inset top-right plots represent the genetic simulations of each migration model. Representative random dispersal from one location to surrounding places; the inset bottom-left plot shows that the Mantel test rejected that gene flow increased with geographic proximity, and Spearman's P -value used. Shading indicates the 95% confidence intervals. A linear regression model with a two-sided test was used for the statistical analysis, and the multiple R-squared was used. **g** Representative directional dispersal, including northward (**h**) and southward dispersal (**i**) from source to destination. All genetic simulations are available in Supplementary Figs. 5 and 6, and Supplementary Table 4. The color gradients of oceans indicate ocean current velocity, and arrows show the directions in summer (**h**) and winter (**i**). Source data are provided as a Source Data file.

source locations, whereas smaller wind drift factors (e.g., 1%) yielded summer dispersal patterns comparable to the contemporary distribution of *T. martensii* (Supplementary Figs. 10 and 11 and Supplementary Tables 6 and 7).

When we simulated the rafting trajectories of each population, we found that the VT population could reach SS within eight months regardless of release timing, whereas SS could only disperse northward to VT during summer (Supplementary Figs. 8 and 9a-c). From the

dispersal trajectories and quantification of dispersal percentage between populations, we found the EB population first connected with South Sulawesi (30.1% reached) and then reached SB (20.2% reached) (Supplementary Table 5), consistent with the close phylogenetic relationship between EB and SS. The quantified ocean current dynamics also showed that transoceanic dispersal from EB to SS owns consistent dispersal direction and higher dispersal velocity compared with land-connected populations (EB and SB) (Supplementary Fig. 9g).

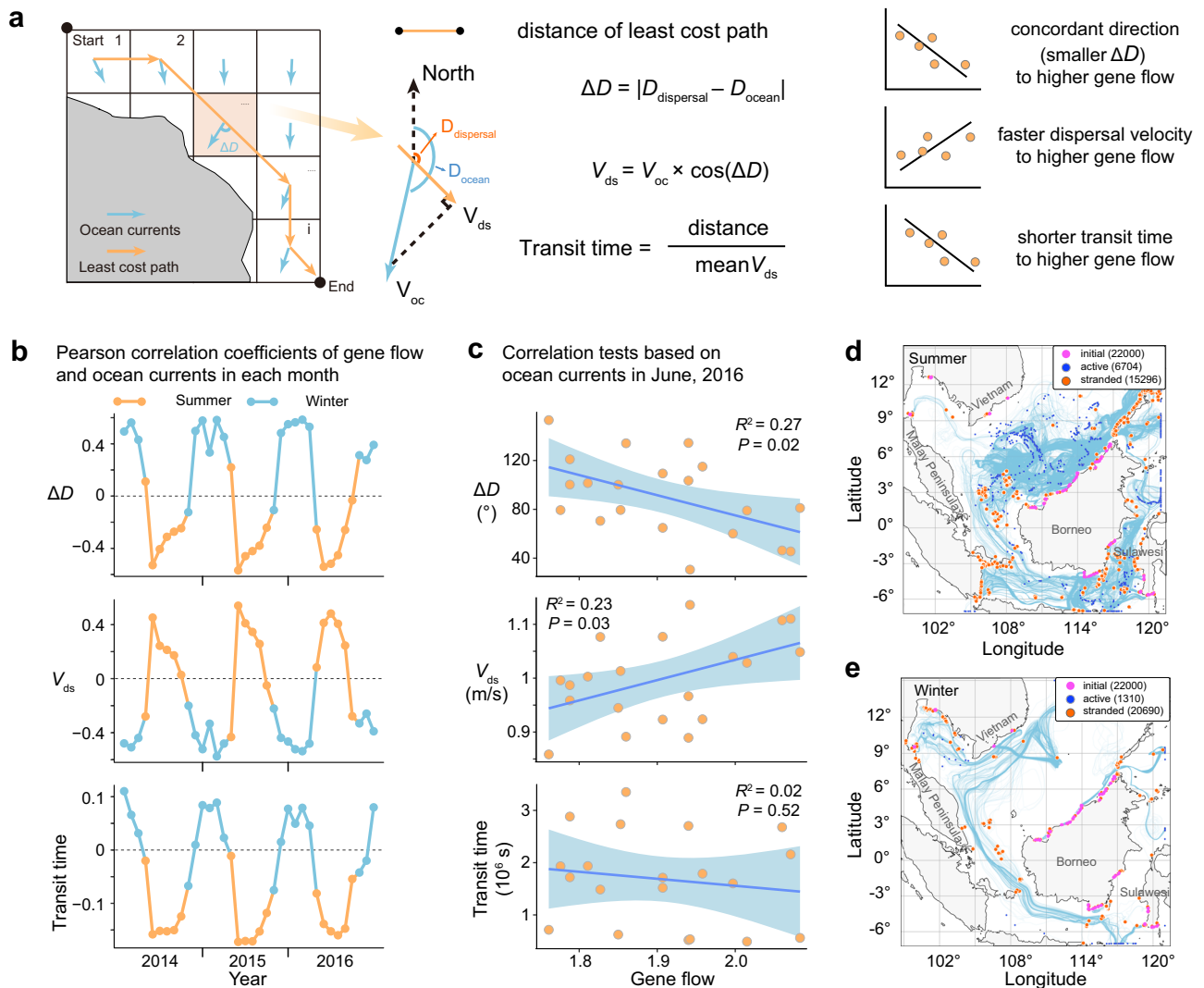


Fig. 2 | Quantified model and particle trajectory simulations suggest summer ocean currents drive asymmetric northward gene flow. **a** Scheme showing quantification of ocean current dynamics between two sites. **b** Pearson correlation coefficients of gene flow and oceanographic dynamics in each month from 2014–2016, including direction deviations between dispersal and ocean currents (ΔD), dispersal velocity, and transit times between sites. **c** Relationship between gene flow and summer oceanographic dynamics in June 2016, including ΔD , dispersal velocity, and transit time between sites. Shading indicates the 95% confidence intervals. A linear regression model with a two-sided test was used

for the statistical analysis, and the multiple R-squared was used. **d, e** Simulated *T. martensii* stranding events (orange circles represent particles that have come into contact with shorelines) and active (blue circles are particles that remain at sea) distribution across the IAA in summer (**d**) and winter (**e**) in 2016. Trajectories are represented as blue lines and were generated using velocity fields from a high-resolution GOEPR ocean model simulation. Particles were recorded every 6 h for eight months after simulated releases from a total of 44 sites (22,000 particles) in 1 April (**d**) or 1 October (**e**). Source data are provided as a Source Data file.

Oceanographic change increases genetic offset

To test how rafting crustaceans will respond to future oceanographic change (in the absence of plasticity), we calculated local, forward and reverse genetic offsets²⁹. Specifically, local offset represents the mismatch between current and predicted future genomic variation in the absence of migration. By contrast, forward genetic offset represents the minimum genetic change a population would experience if migrating to a relatively favorable future location, with high values indicating strong mismatches between contemporary and future genetic compositions. Thirdly, reverse genetic offset seeks to assess whether the genotypes required to adapt to future environments already exist within contemporary populations. To this end, we extracted a total of 117,113 SNPs with minor allele frequency > 10%, to predict genetic offset using the gradientForest (GF) approach, a regression tree-based machine-learning algorithm³⁰.

The ranked importance of environmental variables based on GF analysis indicated that genomic variation in *T. martensii* was strongly associated with sea surface salinity, which shows increasing fluctuation with climate warming (Supplementary Fig. 12). In our analysis, we found that populations in South Sulawesi, south Borneo, the coast along the Gulf of Thailand, and many of the areas along the dispersal route exhibited higher local, lower forward, and higher reverse genetic offsets, except the northern Vietnam range (Fig. 3a–c, Supplementary Fig. 13 and Supplementary Table 8, Supplementary Data 2–4). By analyzing the dispersal potential and forward genetic offsets, we found that increased dispersal distance could mitigate large-scale maladaptation, as most populations will experience reduced habitat suitability if dispersal distances decrease to 100 km (Supplementary Fig. 13e–g and Supplementary Data 3). According to the prediction with unlimited dispersal (Fig. 3b), the future suitable niche for 98.55%

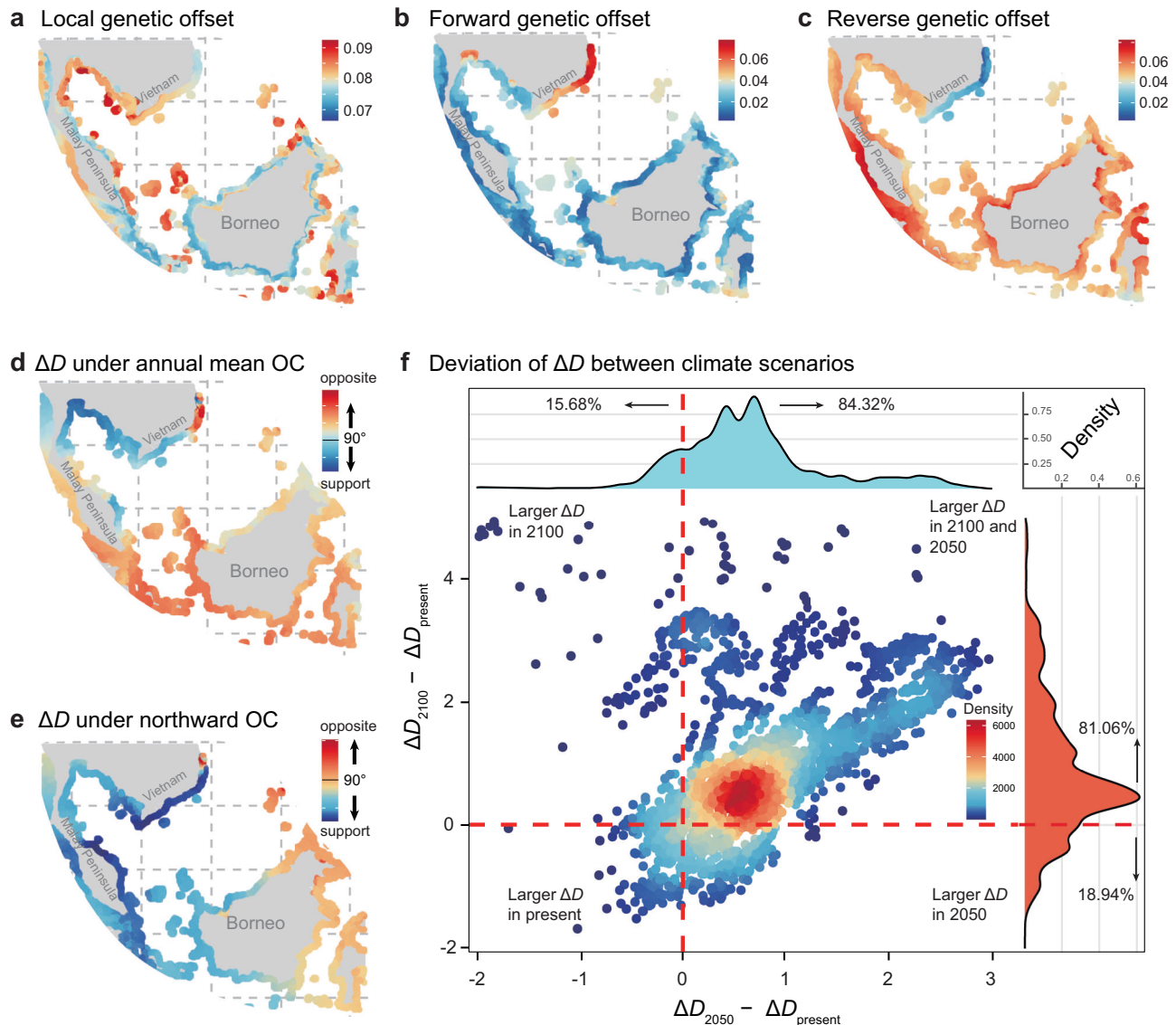


Fig. 3 | Predicted genetic offsets and dispersal risk under future oceanographic changes. **a** Gradient Forest analysis predicted local genetic offsets under 2100 SSP5-8.5 in *T. martensii* ($n = 22,640$ grids). The color scale from blue to red indicates increasing genetic offset values. **b** Predicted forward genetic offsets show populations in most regions have lower genetic offsets with unlimited dispersal distance, except for populations in northern regions. **c** Predicted reverse genetic offset shows that lower genetic offsets were found in northern regions of the species' distribution range. **d** Integration of mean annual ocean current (OC) dynamics and

forward genetic offset suggests 86.95% of populations will experience ΔD values $> 90^\circ$ under 2100 SSP5-8.5, indicating increased difficulty tracking their suitable niche. **e** Based on seasonal northward ocean currents, 80.35% of populations will experience $\Delta D < 90^\circ$. **f** Density plot showing the deviation of ΔD between present and future northward ocean currents under different climate scenarios. About 80% of populations have a larger ΔD to suitable habitats driven by future ocean currents compared with the present, indicating increased difficulty tracking their suitable habitat. Data are provided in Supplementary Data 2–6.

of populations is located north of their current distributions (a total of 22,640 grids; Supplementary Data 4).

Northward rafting supports habitat tracking but dispersal deviations increase

Based on the GF results, we integrated forward genetic offset with ocean current modeling to calculate directional deviation (ΔD) between ocean currents and least-cost dispersal paths, to assess rafting potential of *T. martensii* to suitable habitats. In the absence of land barriers, the least-cost path was calculated as the Euclidean distance between two sites. By contrast, when this path was interrupted by land barriers, the least-cost path was inferred from oceanographic connectivity. Based on annual mean ocean current data under 2100 SSP5-8.5 scenarios, we found that 86.95% of populations will face dispersal-direction deviations (ΔD) exceeding

90° , preventing them from reaching suitable future habitats (Fig. 3d, Supplementary Fig. 14 and Supplementary Data 5). Given that currents in the IAA are predominantly southward, but with strong seasonal variation (northward flow in summer and southward flow in winter), we further tested the species' dispersal potential using seasonal northward ocean current data under present, 2050, and 2100 SSP5-8.5 scenarios. The results suggest that contemporary conditions facilitate northward dispersal in 81% of populations ($\Delta D < 90^\circ$) (Fig. 3e, Supplementary Fig. 15 and Supplementary Data 6). However, compared to present ocean current conditions, 84% of populations under the 2050 SSP5-8.5 scenario show increased ΔD (63% with slower dispersal velocity and longer transit time), while 81% of populations under the 2100 SSP5-8.5 scenario show similar trends (44% with slower dispersal velocity and with longer transit time) (Fig. 3f and Supplementary Fig. 16).

Genetic changes associated with salinity shifts

Salinity shifts pose osmotic challenges to rafting species^{31,32}. Accordingly, we found sea surface salinity to be strongly associated with genomic variation in *T. martensii*, with a total of 575 significant salinity-associated SNPs, located within 459 genes, consistently identified across multivariate latent-factor mixed model (LFMM)³³, univariate LFMM, and redundancy analysis (RDA)³⁴ (Fig. 4a and Supplementary Fig. 17a). Enriched genes included those involved in plasma membrane (77 genes, GO:0005886), ion transport (five genes, GO: 0006811) and SLC-mediated transmembrane transport (19 genes, R-DME-425407) (Supplementary Table 9).

We then performed selective sweep analysis to detect selective signals between the VT population, which experienced the lowest salinity, and the SS population, which faced the highest salinity (Supplementary Fig. 17b). Based on the top 5% F_{ST} and $\theta\pi$ ratio, we identified 126 genes with selective signals in the VT group, and 53 genes in the SS group (Fig. 4b). Many of these genes are similarly implicated in osmoregulatory pathways, e.g., plasma membrane (10 genes, GO:0005886); transmembrane transport (four genes, GO:0055085); potassium ion transport (two genes, GO:0006813) (Supplementary Table 10). For example, *GRIK2*, a glutamate-gated ion channel gene that is known to maintain ionic homeostasis in euryhaline fish³⁵, showed striking associations with salinity ($P = 3.164e - 5$) (Fig. 4c and Supplementary Fig. 18a). We used BLASTp to detect 1:1 orthologs in the genomes of 11 additional amphipod taxa, encompassing a variety of freshwater, marine and terrestrial habitats. Phylogenetic analysis revealed that these *GRIK2* sequences clustered strongly by habitat type (freshwater; marine; terrestrial) rather than reflecting the underlying species phylogeny (Supplementary Fig. 18b), providing further support for this gene's role in amphipod salinity adaptation.

Plastic expression of osmoregulatory genes

To further detect the expression patterns related to salinity shifts, we designed salinity stress experiments for *T. martensii*, and sequenced transcriptomes from the whole body, gills and legs across four salinity gradients (5, 10, 20, and untreated 35 ppt), and five duration gradients (24, 48, 72 h, 15 days, and 30 days) (Fig. 4d). Measurements of hemolymph osmolality reveal significant osmolality differences between salinity gradients (Fig. 4e).

The expression cluster analysis suggests a clear divergence between gills and legs (Supplementary Fig. 19a). According to the differentially expressed genes (DEGs) and gene enrichment analysis between 5 ppt and 35 ppt treatments, the top 10 GO pathways in gills are primarily related to osmoregulation (Fig. 4f and Supplementary Tables 11, 12). Notably, pathways such as amino acid transmembrane transport (five genes, GO:0003333), potassium ion transport (four genes, GO:0006813), and cell volume homeostasis (three genes, GO:0006884) were differentially expressed exclusively in gills rather than legs. Thus, we propose that amphipod gills may be crucial osmoregulatory organs, with a comparable differential expression pattern between tissues also detected in the terrestrial talitrid, *M. aosen* (Supplementary Fig. 19b).

Comparisons between salinity treatments revealed that the number of DEGs increased as treatment duration increased from 24 h to 15 d and 30 d, and also as salinity decreased to 10 and 5 ppt (Fig. 4g). These dynamic expression changes highlight transcriptional plasticity³⁶ (Fig. 4g–i and Supplementary Fig. 19c–f), with the stronger shifts linked to the larger salinity shifts (Fig. 4k) and longer treatments (Fig. 4l).

To further test for salinity plasticity relevant to long-lived natural rafting voyages, we undertook extended stress experiments lasting for 15 and 30 days. Relatively strong expression shifts were detected at low salinities (Fig. 4h) and over the longest treatments (Fig. 4i). Moreover, the number of genes enriched in ion channel transport pathways

increased as treatment time increased (Fig. 4j, Supplementary Table 13). Specifically, the V-type H⁺ ATP genes related to proton transport showed decreased expression with increasing treatment duration (*VATA*, *VATB*, *VATE*, *VATG*, *VATO*). Notably, genes involved in the transport of small molecules (*Tret1*, *ABCA3*, *HXT1*) and inorganic ions (Sodium/hydrogen exchanger, Sodium/Potassium/Chloride Transporter and *KCAB2*) showed increased expression in these treatments (Fig. 4m, Supplementary Fig. 20 and Supplementary Table 14).

Genomic adaptations to driftwood feeding

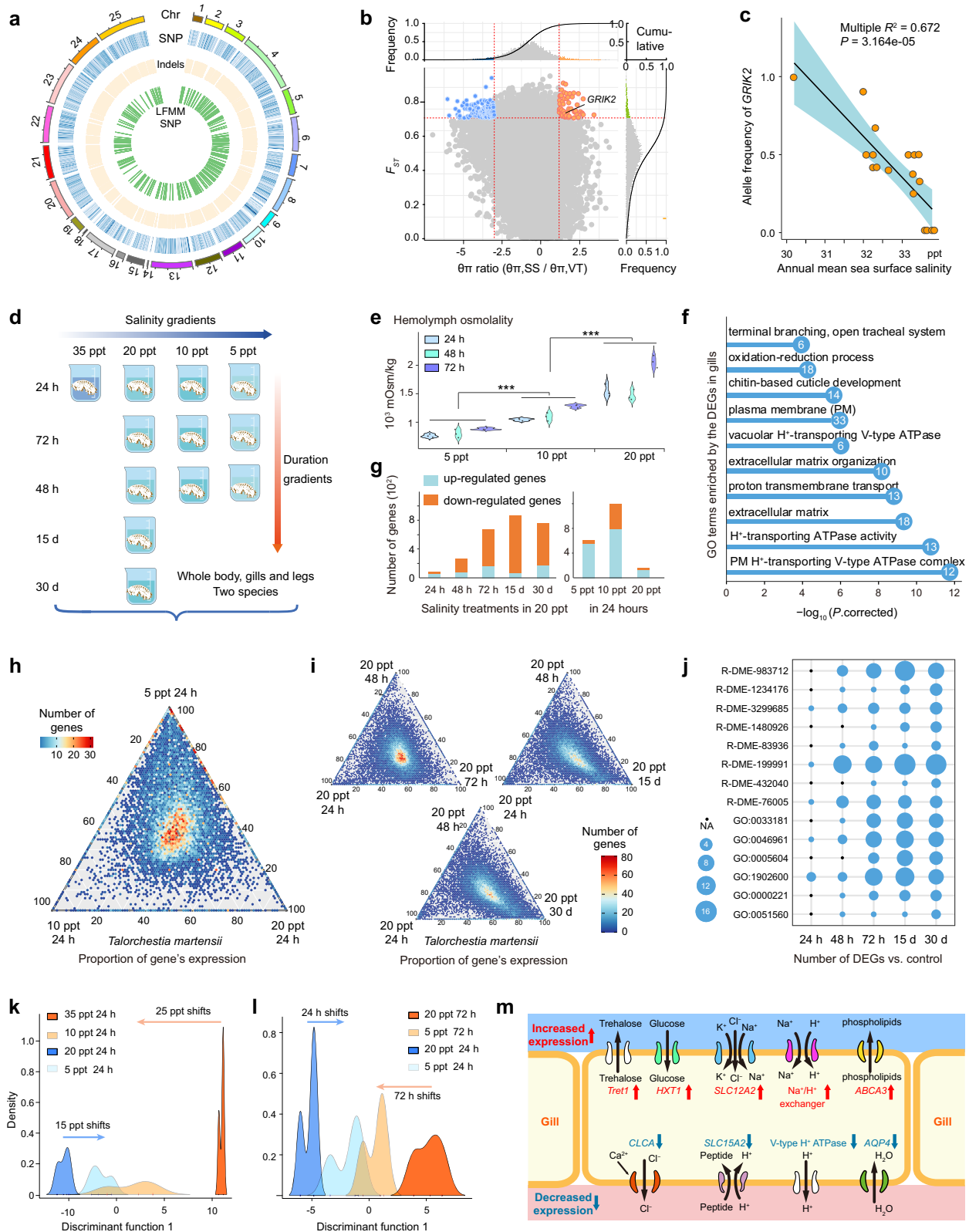
To test for additional genomic adaptations enabling long-distance rafting events on driftwood, we focused on the lignocellulose digestion process (from cellulose to glucose³⁷) (Fig. 5a) that is hypothesized to be essential for wood-feeding taxa. We first constructed a phylogenomic tree for six rafting and three non-rafting amphipod species (Fig. 5b), and identified genes involved in lignocellulose degradation mediated by Carbohydrate-Active Enzymes (CAZymes)³⁸ including glycosyl hydrolases (GHs), carbohydrate esterases, auxiliary activities, along with associated carbohydrate-binding modules and glycosyl transferases. The CAZyme family composition was largely conserved between rafting and non-rafting species; however, the copy number of CAZyme genes varied notably (Supplementary Fig. 21). In particular, rafting species exhibited significantly higher proportions of GH genes compared to non-rafting species (Wilcoxon signed-rank test, $P = 0.044$) (Fig. 5c and Supplementary Table 15).

Gene identification revealed 139 gene copies in the *T. martensii* genome that can be classified into 39 GH families. Three of GHs participate in major steps of wood digestion: (1) Glycoside hydrolase family 9 (GH9) encodes β -1,4-endoglucanases (EC 3.2.1.4) that break cellulose (crystal) bonds to produce individual cellulose polymers; (2) GH7 encodes β -1,4-exoglucanases (EC 3.2.1.91) that cleave cellulose polymers from either end to produce 2-4-mer subunits; and (3) the GH30_1 family encodes β -glucosidases (EC 3.2.1.21) that break cellobiose (glucose 2-mer) into glucose units³⁷ (Fig. 5a).

The gene family expansion and extraction analysis suggest that the GH7 gene family show significant expansion in the rafting species compared with non-rafting species (Fig. 5b and Supplementary Data 7). Phylogenetic analysis shows that crustacean GH9 and GH30_1 gene families are closely related to insect genes, while the monophyletic crustacean clade (including nine talitrids and non-talitrid crustaceans) of GH7 is a sister clade to fungi, suggesting it likely originated from fungi via horizontal gene transfer (Fig. 5d, e).

By comparing the species tree of the nine talitrids with the gene trees of GH proteins, we identified two gene duplication models in the evolution of these genes (Fig. 5d): one within rafting talitrids (Model I), and another at the talitrid ancestor, including non-rafting talitrids (Model II). The GH30_1 gene family consists of three talitrid clades and non-talitrid relatives (Fig. 5e), with six duplication events of Model II and three of Model I. The GH9 gene clade includes three groups: two containing both talitrids and non-talitrids, and one exclusive to talitrids. Among these, two duplications belong to Model I and seven to Model II. For the GH7 family, five duplications are in Model I and four in Model II (Fig. 5e).

To detect the potential function difference between these copies, we compared gene expression, protein sequences and structure generated by gene duplication. Using Clade II of the GH7 gene family as a case study, we found some amino acid variations in different duplication events (Fig. 5e). Protein structure analyses suggest these copies share broadly similar structures (Supplementary Table 16). Moreover, transcriptome analysis revealed that GH7, GH9, and GH30_1 gene copies are highly expressed in the gut, with comparable expression levels in rafting species despite their greater gene copy numbers relative to non-rafting species (Fig. 5f and Supplementary Fig. 22).



Discussion

Summer ocean currents drive the asymmetric northward gene flow and rafting

The phylogeographic patterns detected in this rafting talitrid outwardly appear to conform to the biogeographic expectations of Pleistocene sea-level fluctuations^{39–41} and Wallace’s Line^{42–44} (Supplementary Note 1). During the early Pleistocene, sea-level decline

exposed the Sundaland landmass, connecting the coastlines of Vietnam-Thailand and Borneo¹⁹, and isolating the VT + SB + NB clade from the EB and SS populations (Supplementary Fig. 4). Subsequent sea-level rise created new intertidal zones around Borneo, enabling coastal talitrids to expand their ranges; the NB and SB lineages likely diverged from VT around 1.78 Ma. A subsequent split between NB and SB at ~0.66 Ma aligns with sea-level fluctuations during the

Fig. 4 | Genetic changes in *T. martensii* associated with osmoregulation promote rafting acclimations to salinity shifts. **a** Circos plot of *T. martensii* genomic features showing 25 large scaffolds, distributions of SNP, Indels, and SNP inferred by LFMM based on a 50-kb sliding window. **b** Selective sweep analysis of the South Sulawesi population (SS, high salinity exposure) and Vietnam-Thailand population (VT, low salinity exposure). Data points located above the upper 5% tail of the F_{ST} distribution, and the left and right of the 5% tails of the θ_{π} ratio distribution were identified as selected regions. **c** Negative relationships between the allele frequency of SNP in *GRIK2* and annual mean sea surface salinity. Shading indicates the 95% confidence intervals. A linear regression model with two-sided test was used for the statistical analysis, and multiple R-squared was used. **d** Gradient salinity stress experiments for coastal *T. cf. martensii* and terrestrial *M. aosen*. **e** The measured hemolymph osmolality suggests a significant difference between salinity gradients. Each box were obtained from three replicates. Statistical significance was assessed using the two-tailed Mann-Whitney U test: *** indicates $P < 0.001$. **f** The top 10 GO enrichment

pathways for the upregulated expression genes in gills. Values in the circle represent the gene number. **g** The number of DEGs changed along the salinity and duration gradient treatments. **h** Ternary plots depicting the higher proportion of gene expression at 5 ppt than 10 and 20 ppt. **i** Ternary plots depicting the proportion of gene expression increased along the duration from 72 h to 15 d and 30 d compared with 24 h and 48 h. **j** The number of genes that enriched in ion channel transport pathways along the treatment duration. e.g., R-DME-983712: Ion channel transport; GO:1902600: proton transmembrane transport; details in Supplementary Table 13. **k, l** Discriminant analysis of principal components (DAPC) indicates gene expression plasticity in response to salinity shifts over the same duration (**k**) and duration changes under the same salinity (**l**). **m** Hypothesized model of ion transport across the gill based on genes with increased (red) and decreased (blue) expression over duration gradient treatments. Source data are provided as a Source Data file.

Naynayxungla Glaciation (0.78–0.50 Ma)⁴⁰, when land bridges between the Malay Peninsula and Borneo likely drove regional isolation. In addition to historical sea-level fluctuations, Wallace's line has long been regarded as a barrier for marine and terrestrial species in the IAA^{42,43}, even for species with extended pelagic larval dispersal⁴⁴. In our study, the relatively deep genetic split between SS + EB and VT + SB + NB implies that modern oceanographic circulation in IAA has failed to fully erase these historical biogeographic patterns. Nevertheless, our analyses provide evidence of ongoing rafting-mediated gene flow between populations across the region (Fig. 1e, f).

Oceanographic currents provide a plausible explanation for this asymmetric northward gene flow (Fig. 6a). Crucially, during the boreal summer, surface water from the Java Sea enters the South China Sea through the Karimata Strait and flows northward along the Malay Peninsula coast, and eventually joins the northeastward Vietnam Coast Current^{18,20}. Quantitative ocean current dynamics revealed that northward ocean currents in summer exhibit significant concordance with observed gene flow patterns, which enhanced northward dispersal (Fig. 2a–c).

Particle trajectory simulations provide a powerful tool in rafting dispersal studies^{45,46}. By using drifting particles that lack mass or volume, such simulations carry the advantage of reducing computational complexity. However, the hydrodynamics of real driftwood fragments may be strongly influenced by parameters such as mass, volume, density and water density⁴⁷. By comparing “wind_drift_factors” of 1% to 3%, we found that large driftwood pieces often strand near their source locations, whereas smaller driftwood fragments more readily disperse between islands of IAA (Supplementary Figs. 10 and 11). Moreover, by integrating salinity and temperature variables with these complex particle models, our simulations revealed a substantial increase in successful rafting between SS and VT (14.6%) than did comparable winter simulations (0.7%) (Fig. 2d, e).

A key characteristic of dispersal driven by ocean currents is that the similarity among populations is more strongly correlated with marine connectivity than with geographic distance. Along these lines, phylogeographic analysis indicates that the EB population is more closely related to the transoceanic SS population than to the land-connected SB population. Both quantified ocean dynamics and particle trajectory simulations suggest that transoceanic rafting between EB and SS is facilitated by concordant dispersal directions and higher velocities, leading to stronger gene flow and a closer relationship between transoceanic populations compared to the land-connected populations (Supplementary Fig. 9).

These results demonstrated the northward ocean currents in summer contributed to the asymmetric northward gene flow and maintaining genetic connectivity between populations in the IAA (Fig. 6a). Furthermore, the quantified ocean dynamics simplify the species dispersal as the shortest path between two sites, and calculate the ocean currents variables on this path to explain their relationship

with gene flow²⁶. The mutual corroboration among analyses suggests that quantified ocean dynamics represent a promising tool for revealing correlations between ocean currents and rafting dispersal.

Marine rafting species may require high genomic variation to adapt to future salinity changes

Despite the importance of rafting processes in marine ecosystems, few previous studies have combined rafting and genomic forecasting in the evaluation of future dispersal potential⁴⁸. Genetic offsets are measures of environmental ‘distance’ that correlate most strongly with genetic structure, as highlighted by recent analysis of marine invertebrates⁴⁹, migratory birds^{50,51}, and fishes⁵² to evaluate the climate maladaptation. Genetic offsets show the instantaneous degree of maladaptation of a genome when moved to new environments^{53,54}. While such offset analyses are yet to fully account for organismal plasticity, the substantial population genomic structure detected here in *T. martensii* highlights the importance of local adaptation in this rafting species. As a case in point, we found that osmoregulatory loci (e.g., *GRIK2*) exhibit strong allele frequency shifts linked to salinity gradients⁵⁵. These results also revealed signatures of local adaptation in rafting species despite their high dispersal potential, which align with previous studies of other high-dispersal marine species, such as *Strongylocentrotus purpuratus*⁵⁶, *Chlorostoma funebris*⁵⁷, and *Semibalanus balanoides*⁵⁸. These signatures of natural selection further highlight the need for adaptive responses under future climatic and oceanographic change scenarios⁵⁹ (Fig. 3a–c), which are projected to increase levels of salinity fluctuation (Supplementary Fig. 13d).

Under global change, rafting is likely to present a key mechanism for many marine species tracking their shifting habitats. Along these lines, northward dispersal of *T. martensii* could potentially mitigate the projected genomic maladaptation of this species under future oceanographic scenarios (Fig. 3b and Supplementary Fig. 13e–g). A wide range of marine species, from phytoplankton to fish and marine mammals, have shown direct evidence of such poleward dispersal under climate warming⁶⁰. Compared to annual mean ocean currents, which oppose northward dispersal, seasonal northward currents may facilitate movement to suitable habitats (Fig. 3d, e). However, nearly 80% of populations will experience increased dispersal direction deviation as climate warming continues (Fig. 3f). These findings highlight that shifting oceanographic conditions can pose challenges for rafting species reliant on passive dispersal¹⁵.

Broadly, while our integrative analyses suggest that *T. martensii* has the potential to disperse and adapt to the thermal and osmoregulatory challenges provided by global change (Fig. 6b), shifting oceanographic connectivity patterns may limit its ability to do so. Given the vast numbers of rafting marine species likely to be impacted by forecast marine climate change, there is also an urgent need for further data to help assess and forecast such biological responses. Genetic offset analysis could be a powerful approach for applied conservation, although

a Process of wood-degrading and associated GH families

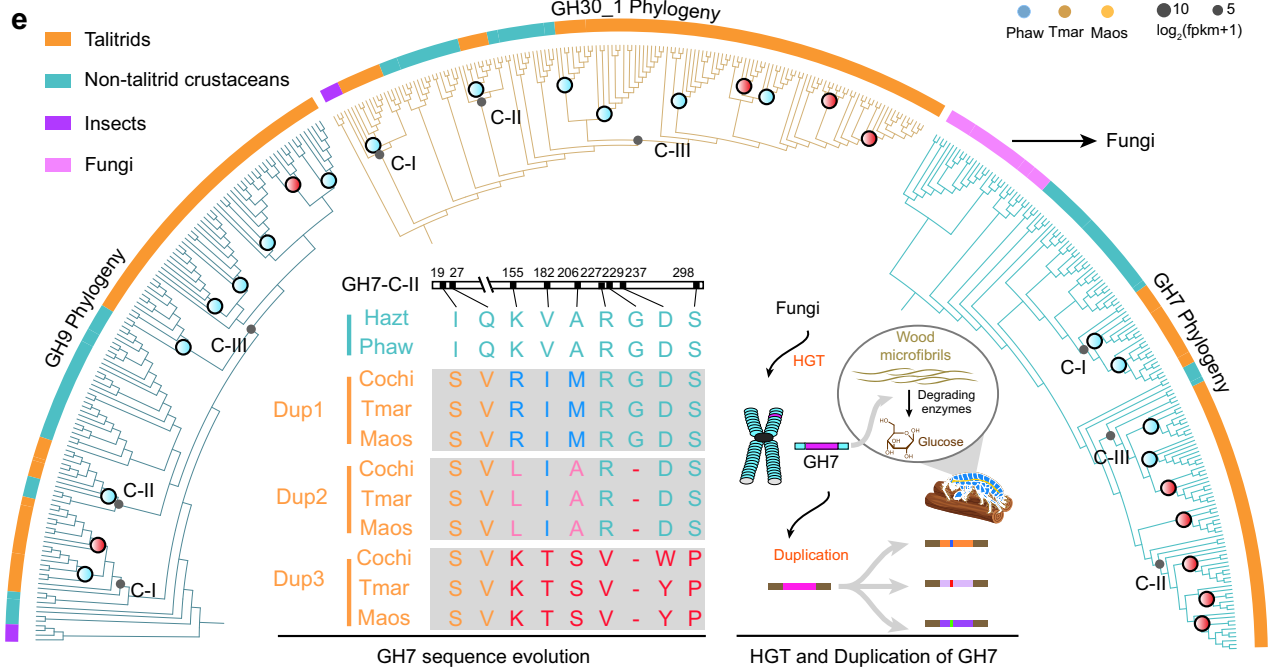
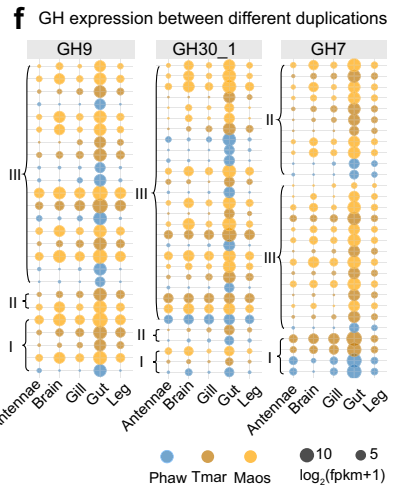
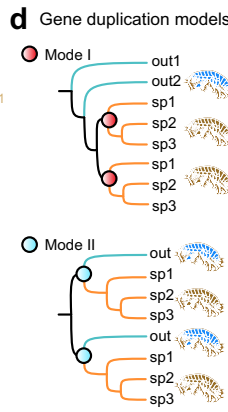
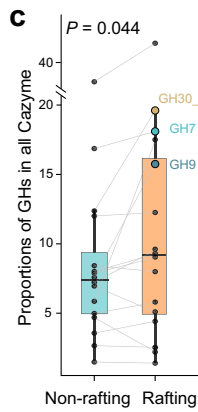
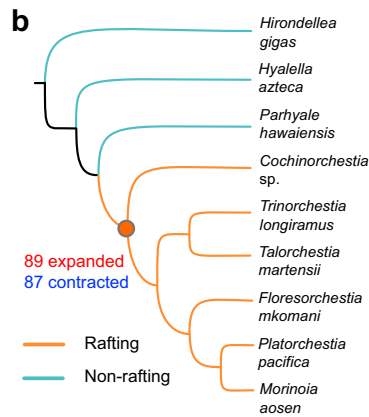
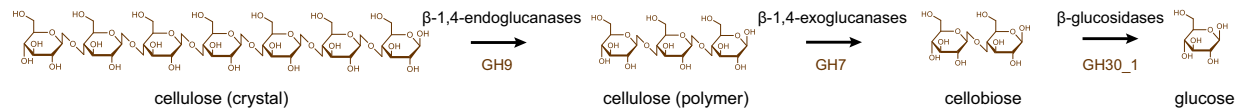


Fig. 5 | Horizontal gene transfer and duplication events of GH gene families. **a** Three major steps of wood-degrading from cellulose to glucose and associated glycoside hydrolase (GH) gene families. **b** The reconstructed phylogeny based on three non-rafting and six rafting amphipod genomes. **c** Comparisons of the proportion of GH gene families in all cazymes indicate that rafting talitrids have more GHs than non-rafting species ($n = 16$). Boxplots indicate the median (center line), the 25th and 75th percentiles (bounds of the box), and whiskers extending to 1.5 × the interquartile range. All individual data points, including values outside the whiskers, are shown. Two-sided paired Wilcoxon signed-rank test P -values are reported on the plot. **d** Two detected duplication modes of the GH gene family in talitrids. **e** The inferred phylogenetic relationships of the GH9, GH30_1, and GH7

proteins from talitrids, non-talitrid crustaceans, insects, and fungi. Circles on the clade represent different duplication models present in (d). Black dots on the nodes correspond to different talitrid clades. The middle left aligned sequences show the amino acid variation of GH7 clade II (C-II) from *Parhyale hawaiiensis* (Phaw), *Hyalella azteca* (Hazt), *Cochinochestia* sp. (Cochi), *Talorchestia martensii* (Tmar), and *Morinoia aosen* (Maos). The middle right schemes show a summary of the GH7 evolution, including horizontal gene transfer (HGT) from fungi to crustacean ancestors and gene duplication in talitrids. **f** the expression patterns of GH7, GH9 and GH30_1 between three species and five tissues. Each line represents one gene copy, and circle size indicates expression level. The black brace and numbers correspond to the clade in Fig. 5e. Source data are provided as a Source Data file.

their correlation with fitness changes in new environments depends on patterns of local adaptation in the metapopulation, the fitness landscape, and other biological responses such as plasticity^{61,62}. We particularly emphasize the need for additional common garden experiments and temporal genomic studies to further inform marine biodiversity change forecasts and potential management actions.

Osmoregulatory plasticity and wood-feeding promotes rafting acclimation
During rafting voyages, salinity shifts can exceed 15 ppt, posing huge osmotic challenges to species dispersing passively at sea. Crucially, shifts in gene expression can facilitate salinity acclimation and enable populations to survive in such dynamic habitats^{63,64}. We found

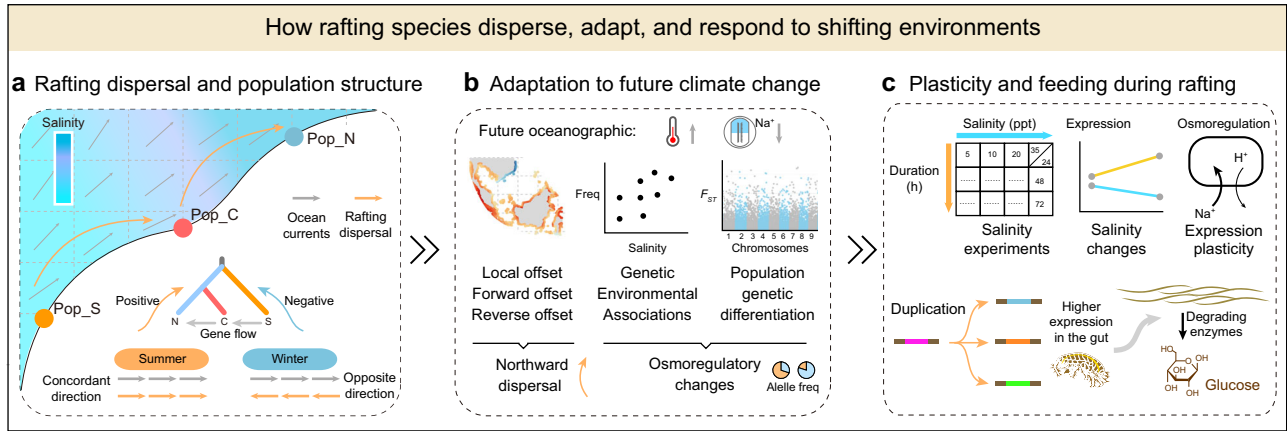


Fig. 6 | Framework of how rafting species disperse, adapt, and respond to shifting environments. **a** Schematic representation of rafting-mediated dispersal between populations. **b** Facing future oceanographic changes (increasing temperature and decreasing salinity), we found northward dispersal and osmoregulatory genetic changes that may facilitate their adaptation to future climate

change. **c** We detected osmoregulatory gene expression plasticity that helps talitrids cope with short-term salinity fluctuation during rafting events, and key gene duplications of wood-degrading enzymes that facilitate energy acquisition during rafting.

increasing differential expression of genes in response to decreasing salinity (Supplementary Note 2), with evidence that gills function as the major osmoregulatory organs in maintaining homeostasis under fluctuating salinity^{64,65}. Rapid gene expression shifts suggest plasticity may be a key prerequisite for successful rafting, at least in the short term⁶⁶ (Fig. 6c). Nevertheless, theoretical studies suggest that, in the longer term, plasticity may slow or constrain populations' adaptive genetic response to environmental stress⁶⁷. Therefore, we propose that both short-term (plastic) responses to temporal environmental variation and longer-lasting adaptive responses to local conditions should be integrated to understand how rafting species may disperse and respond to future climates.

In addition to physiological plasticity, competition for space and food on the driftwood also influences rafting success⁶⁸. The slender morphology of *T. martensii* (<15 mm) likely facilitates their crypsis on and in driftwood, minimizing potential predation by birds or fish⁶⁹. Furthermore, their fecundity (10–20 eggs per female) and rapid generation time likely enhance the survival of rafting populations. Crucially, the ability of this species to feed on driftwood, enables lengthy rafting voyages⁷⁰. In particular, the high proportion of key GH genes that are highly expressed in the gut emphasizes the key role of wood feeding in this rafting system (Fig. 6c).

In summary, our results highlight the diverse physiological and genomic adaptations underpinning the strong rafting ability and adaptive success of coastal marine invertebrates (Fig. 6). This integration of diverse genomic, physiological and environmental data sheds key new light on the adaptability of rafting species in our fluctuating tropical oceans.

Methods

Sample collection and genome sequencing

A total of 203 talitrid samples from 80 localities were collected from the IAA coastline from August 2017 to September 2018. We first performed species delimitation followed Liu et al. (2023)⁷¹ and inferred phylogenetic relationships based on the concatenated dataset comprising the mitochondrial (*COI*, *COII*, 16S) and nuclear (18S rRNA, 28S rRNA, *H3*, *NaK*) gene regions. All the primers were followed by Liu et al. (2023)⁷¹. Then, we collected *T. martensii* specimens (voucher number: T2811) from Gerigat, Sarawak, Malaysia (E 111.20°, N 2.04°) for genome sequencing. We isolated genomic DNA from adult talitrids using a Qiagen Blood & Cell Culture DNA Kit (QIAGEN, Hilden, Germany). We sequenced short-insert paired-end (PE, 150 bp) libraries on the Nova-seq 6000 platform (Illumina). A total of 239.88 Gb clean reads (~370 ×)

was obtained after removing low-quality reads with poor sequencing accuracy and adapters with Trimmomatic v.0.39⁷². Genome assembly and annotation followed the method of Liu et al. (2023)⁷¹. We further scaffolded the contig-level assembly to a pseudochromosome scale with RagTag v2.0.0⁷³ using *Morinoia aosen* (GCA_030386875.1)⁷¹ as a reference.

Talorchestia martensii population resequencing and SNP calling

We used *T. martensii* samples from 44 sampling sites for genome resequencing. The obtained clean reads (average 15 ×) were mapped to the reference genome using BWA v0.7.12⁷⁴. The PCR duplicates of each of the samples were removed with Picard MarkDuplicates (<http://broadinstitute.github.io/picard/>). We used the HaplotypeCaller engine in GATK v3.7.0⁷⁵ to call SNPs from the BAM alignment file for each sample. The option -ERC GVCF was used to convert the variants into gVCF format, and the gVCF of each sample was merged to allow a multi-sample joint genotype procedure using the GATK GenotypeGVCFs engine. For SNPs, we further used VCFtools v0.1.13⁷⁶ and BCFtools v1.9⁷⁷ to remove indels and keep only biallelic SNPs with the following filtering criteria: (1) minQ > 30, (2) read depth > 5, (3) max-missing counts = 5, (4) SNPs at least 5 bp away from indel regions. We further excluded highly correlated SNPs by performing linkage disequilibrium based SNP pruning in PLINK v.1.9.0⁷⁸ with a default pairwise r^2 threshold 0.2. This threshold reduces LD-induced bias while preserving enough independent genetic markers to accurately infer population structure, an approach previously used in marine genomic studies⁷⁹.

Population structure analysis within *T. martensii*

To characterize population structure, we first used SNP data from all samples and constructed phylogenies using RAXML v.8.2.9⁸⁰. Then, we used a PCA implemented in the R package snprelate⁸¹ to identify clusters of individuals. We also conducted genetic structure analysis in ADMIXTURE⁸², which also allowed us to infer individual ancestry proportions. We used default parameters and defined the assumed genetic clusters *K* as ranging from 1 to 13.

Demographic history and gene flow analysis

We inferred the *T. martensii* population dynamics and demographic changes over large timescales with high resolution of different samples using the Pairwise Sequentially Markovian Coalescent (PSMC) method²². We also used the population genetic modeling framework in the program G-PhoCS v1.2.3²³ to estimate the lineage divergence for

the *T. martensii* clade based on SNP datasets. Details about these methods can be found in Supplementary Note 3.

We performed another two analyses to calculate the migration rates and direction between different groups. First, the migration events were inferred using TreeMix²⁴ by assuming zero to five migration edges. Then, to quantify gene flow between different populations, we calculated D-statistics and f₄-ratio statistics with D-suite v0.4⁸³. We considered gene flow to be significant with a *P* value < 0.05 and |Zscore| > 3.

Dispersal hypothesis and gene flow model testing

We used Fastsimcoal 2.7²⁵ to simulate *T. martensii* population migration patterns based on the following dispersal hypotheses: (1) random dispersal from one location to surrounding places without consistent directions, and (2) directional dispersal from source to sink, including (2a) northward dispersal from the southern to northern group, and (2b) southward dispersal from the northern to southern group (Supplementary Fig. 5). The SNP data were converted to site frequency spectrum (SFS) data using easySFS.py (<https://github.com/isaacovercast/easySFS>). We first used five populations (*K* = 5) to infer the potential dispersal hypothesis, and listed 25 models for simulation. The model fitness was evaluated by simulating SFS for each demographic model and comparing the simulated and observed likelihoods. The best demographic model was determined based on the maximum likelihood value. During this process, we found the dispersal hypothesis and model prior could be very complex.

To simplify the model prior, we defined groups based on population structure (*K* = 3), with the EB and SS populations designated as the south group, the SB and NB populations as the central group, and the VT population as the north group. We also listed 20 alternative models for genetic simulation. Among these models, four tested for southward dispersal, four for northward dispersal, and 12 for random dispersal between separate regions. For each model, we carried out 50 runs with 40 expectation-maximization cycles and one million coalescent simulations to simulate migration rates, *N_e*, and divergence time.

Quantification of ocean current dynamics

We developed a quantified model by quantifying the dispersal direction deviation, species dispersal velocity, and transit times between two sites based on the least-cost path and gridded ocean current data (1/12° horizontal resolution). The least-cost path between each pair of individuals was measured using the R package marmap⁸⁴ with bathymetric data from the ETOPO1 database⁸⁵, which is hosted by NOAA. We slightly adjusted some sample positions to avoid samples on land because there was limited resolution of bathymetric data in coastal waters. We identified each grid cell that intersected the least-cost path.

We calculated the direction deviation value (ΔD) between the dispersal route direction ($D_{\text{dispersal}}$) and ocean current direction (D_{ocean}) in the least-cost path from source to destination.

$$\Delta D = |D_{\text{dispersal}} - D_{\text{ocean}}| \quad (1)$$

ΔD is a score between 0 and 180°, where greater than 90° indicates that the ocean current direction of the grid cell is inverse to the dispersal path connecting the populations. We then used the averaged values across all grid cells of the path as direction deviations between sites.

Then, we calculated the dispersal velocities (V_{ds}) for each grid cell according to the gridded velocities of ocean currents (V_{oc}) and direction deviation value (ΔD) of the least-cost path:

$$V_{ds} = V_{oc} \times \cos(\Delta D) \quad (2)$$

The dispersal velocities between sites were calculated as the averaged value of all grid cells on the least-cost path. Finally, the transit times were calculated as distance/velocity between sites.

$$\text{Transit times} = \frac{\text{Least cost distance}}{\text{mean } V_{ds}} \quad (3)$$

Ocean current dispersal trajectory simulations

We used an individual-based Lagrangian particle trajectory model²⁶ to predict the possible trajectories and stranding events of passively drifting individuals. The passive drift trajectories of individuals were computed using the OceanDrift model implemented in the Python-based Lagrangian trajectory simulation framework OPENDRIFT.

To investigate the influence of environmental variables on the rafting pathways, we used the PelagicEggDrift model and added the environmental temperature and salinity into the simulations. We recorded the stranded locations and calculated the percentage of particles reached each region to evaluate population connectivity quantitatively. We used modeled surface current fields and sea water temperature and salinity from Global Ocean Ensemble Physics Reanalysis (GOEPR), which was developed by the Copernicus Marine Environment Monitoring Service (CMEMS; <https://marine.copernicus.eu/>). As we collected most of the samples during 2017, we used GLORYS12V1 ocean current data (1/12° horizontal resolution) over three years (January 2014–December 2016) as input to account for seasonal variation in oceanographic dynamics.

While driftwood typically follows currents, the shape and mass of these particles influence their buoyancy and sensitivity to wind slippage. Therefore, to investigate the effects of driftwood mass and shape, we changed the value of “wind_drift_factor” (1%, 1.5%, 2%, 2.5%, 3%) in our passive ocean surface drift model. The ocean–wind variables were obtained from the global atmospheric model from the National Centers for Environmental Prediction (NCEP; <https://www.ncep.noaa.gov>).

We ran general drift simulations using 500 particles randomly distributed within a 3 km radius around the central coordinates of each collection site. In total, 22,000 particles were released from 44 sites, representing the full extent of the current *T. martensii* distribution. As seasonal monsoons in IAA shift ocean current direction and talitrid have an eight-month life cycle, in this study, we set two releasing dates as 1 April and 1 October for passive drift simulation in summer and winter, respectively. We simulated each drifting process for a conservative eight-month period and recorded the trajectories hourly for the dispersal trajectory plot.

Identification of genomic variants associated with salinity adaptation

To identify the environment-associated variants across the whole genome, we retained SNPs with a minor allele frequency > 10%, which refers to alleles that are common enough to be reliably for the detection of traits associations⁵⁰. We obtained the present oceanographic data of the four annual mean environmental variables (sea surface temperature, sea surface salinity, ocean current direction, and ocean current velocity) from Bio-ORACLE (<https://www.bio-oracle.org/>). To constrain the species distribution near the coastal area, we added the variable “distance from shore” from the MARSPEC database (<http://marspec.weebly.com>) for environment analysis⁸⁶. To obtain a more accurate comparison of climate influence, we used Z-Score standardization methods $X' = (X - \mu) / \delta$ to scale the climate variables, while *X* is original value, μ is mean of the original data, δ is standard deviation of the original data, and X' is the scaled standardized value.

Based on the SNP data and oceanographic variables, we first calculated the weighted *R*² value for each climatic variable to assess its importance and selected the top variables by ranking their importance

as the major environmental variables for further analysis. Then, we used the turnover function in GF models to convert complex climate data into patterns of genetic variation (allele frequencies), subsequently to select and weight these variables to best summarize genomic variation.

To identify environment-associated variants across the whole genome, we first used the multivariate LFMM2, univariate LFMM implemented in the R package LEA v3.12.2⁸⁷ separately to search for associations between environmental variables and allele frequencies. Based on the five ancestry clusters inferred with ADMIXTURE, we ran univariate LFMM with five latent factors to account for population structure in the genotype data. For each environmental variable, we ran five independent MCMC runs using 5,000 iterations as burn-in followed by 10,000 iterations. *P* values from all five runs were then averaged for each variant and adjusted for multiple tests using a false discovery rate correction of 5%. Second, we performed RDA using the R package *vegan* to identify genetic variants showing an especially strong relationship with multivariate environmental axes⁸⁸. Environment-associated variants were identified as significant if their loading value was greater or less than three standard deviations above or below the average value.

Genetic offset modeling under future climate scenarios

Based on the identified environment-associated SNPs, we used the gradient forest models to calculate the genetic offset and predict how allele frequencies would shift under future oceanographic change. The future climate data [2040–2050 (2050) and 2090–2100 (2100)] of the environmental variables were obtained from Bio-ORACLE. Two shared socioeconomic pathway (SSP) scenarios were applied: SSP1-2.6 and SSP5-8.5. To estimate the spatial regions where the genotype–environment relationship will be most disrupted under future oceanographic conditions, we transformed the oceanographic variables from each of the four climate scenarios (2050 SSP1-2.6, 2100 SSP1-2.6, 2050 SSP5-8.5, and 2100 SSP5-8.5) into genetic importance and calculated the Euclidean distance between the present and future genomic importance values for each grid, which served as a metric of genetic offset.

Following the methods in Gougherty et al., 2021²⁹, we integrated migration to predict potential maladaptation to future oceanographic change and calculated three different forms of genetic offset by the gradientForest approach: the local offsets for each climate scenario, and forward and reverse genetic offsets for 2100 SSP5-8.5. To assess the sensitivity of dispersal constraints, we tested how forward offset varied under migration limits of 100, 500, 1000 km, and unlimited dispersal within the IAA marine ecoregion.

As the GF algorithm and forward genetic offset methods can estimate the target location of species dispersal, we integrated the quantified ocean dynamics with forward offset prediction to test whether the ocean currents can support such dispersal. Based on the future suitable location estimated by forward genetic offset with unlimited dispersal under 2100 SSP5-8.5 scenarios, we calculated ΔD , dispersal velocity, and transit times needed to that location caused by annual mean ocean currents and the northward ocean current dynamics. Finally, we compared ΔD , dispersal velocity, and transit time differences between present and future climate scenarios by subtracting present values from future values.

Selective sweep analysis between populations

We defined the salinity of seawater surrounding each collection site as their salinity exposure and chose two populations with the most dramatic salinity exposure differences to test the selection signals related to salinity adaptation. We used a sliding window method (50 kb windows with 25 kb increments) to calculate the genome-wide distribution of the $\theta\pi$ ratios ($\theta\pi_{\text{high salinity}}/\theta\pi_{\text{low salinity}}$) and F_{ST} values between population pairs. The windows with significantly low and high

$\theta\pi$ ratios (lowest 5% regions and top 5% regions) and significantly high F_{ST} values (top 5% regions) were selected as regions with strong selection signals along the genome. We defined the candidate genes under selection as those within or overlapping with regions showing selective sweeps. The Gene Ontology and Reactome pathway enrichment analysis was implemented in KOBAS 3.0 using Fisher's exact test ($P < 0.05$) with *Drosophila melanogaster* as a reference⁸⁹.

Salinity stress experiments and expression plasticity analysis

To test talitrids' genetic responses to salinity shifts during rafting events, we cultured adults of the coastal talitrid *Talorchestia cf. martensii* and terrestrial talitrid *Morinoia aosen* in different salinity seawater and evaluated the expression changes of selected genes. For coastal *T. cf. martensii*, we set four salinity gradients (35 ppt as control, and 20, 10, 5 ppt) with three duration gradients (24, 48, and 72 hours). To investigate the long-term expression changes of *T. cf. martensii*, we also treated the talitrids in 20 ppt for 15 and 30 days. For terrestrial *M. aosen*, we set four salinity gradients (5, 10, 20, 35 ppt) with three duration gradients (24, 48, and 72 h), using terrestrial treatment as control. To detect the hemolymph osmolality difference between different treatments, we measured the hemolymph osmolality with a Fiske 210 Micro-Sample Osmometer (Advanced Instruments). The hemolymph was collected from 10–15 individuals using a micro-capillary tube to extract fluid from between the second and third abdominal. All data were obtained from three replicates.

Whole body RNA from a single individual and tissue RNA from a mixture of tissues from 10–15 individuals was extracted using the RNAsimple Total RNA Kit (TIANGEN, Beijing, China). RNA-seq was performed on the NovaSeq 6000 platform, and we obtained at least 6-Gb clean data from each transcriptome after removing reads containing adapter, ploy-N, and low-quality reads. All data were obtained from three replicates in each assay. The expression level (fragments per kilobase million) of each gene was calculated with RSEM v1.3.3 and log-transformed ($N + 1$) following quantile normalization⁹⁰.

Differentially expressed genes (DEGs) between different salinity and duration gradients were identified using “DESeqDataSetFromMatrix” and “DESeq” functions in the R package DESeq2 v1.24.0⁹¹. The threshold value of DEGs was set to *P*-value < 0.05 and absolute of fold change ≥ 2 . $\log_2(\text{FC}) \geq 1$ indicates up-regulation, and $\log_2(\text{FC}) \leq -1$ indicates down-regulation.

The DAPC approach was used to compare the expression of DEGs using the R package *adegenet*⁹². The gene expression plasticity in response to salinity and duration gradients was quantified as the magnitude of the shift away from the reference points.

Genetic changes related to wood-feeding in *T. martensii* and talitrids

We searched for GH family proteins in the *T. martensii* genome and eight other talitrids using the Carbohydrate Active enZymes (CAZy) database (dbCAN), which uses hidden Markov models to define the signature domains for each CAZy family⁹³, including *Hyaella azteca* (GCA_000764305.4)⁹⁴, *Parhyale hawaiiensis* (GCA_001587735.2)³⁷, *Hirondellella gigas* (CNCBdb Project ID CNP0005374)⁹⁵, *Trinorchestia longiramus* (GCA_006783055.1)⁹⁶, *Morinoia aosen* (GCA_030386875.1)⁷¹, *Floresorchestia mkomani* (SRR23898670 under PRJNA938803)⁷¹, *Cochinorchestia* sp. (SRR23898667 under PRJNA938803)⁷¹, *Platorchestia pacifica* (SRR23898669 under PRJNA938803)⁷¹. We analyzed all predicted proteins in the genome using HMMER v3.1b2⁹⁷ with an E-value threshold of $1e - 5$.

To assess the molecular evolution of the GH gene family, we identified GH7, GH9, and GH30_1 protein sequences in all eight talitrids. To further verify the protein sequence variations, we predicted the protein structure based on the all GH7 amino acid sequences on the SWISS-MODEL online website (<https://swissmodel.expasy.org/>). Moreover, we obtained these protein sequences from other organisms by a

BLASTp search of the GenBank non-redundant protein database using the sequences identified in the talitrid species as query sequences. We constructed a phylogenetic tree with these three proteins separately with the PROTGAMMALG substitution model using RAxML.

To compare the genomic difference between rafting and non-rafting species, we used OrthoFinder v2.5.4 to define gene families based on protein-coding genes⁹⁸. Gene family expansion and contraction analyses were performed using CAFE v4.2⁹⁹.

Reporting summary

Further information on research design is available in the Nature Portfolio Reporting Summary linked to this article.

Data availability

All the raw RNA-seq (SRR34777140, SRR34777151–SRR34777186, SRR34777191, SRR34777202, SRR34777213, SRR34777215–SRR34777246, SRR34777256, SRR34777267, SRR34777278, SRR34777289, SRR34777300, SRR34777311–SRR34777313, SRR36240034–SRR36240062), and genome resequencing data (SRR34777130–SRR34777139, SRR34777141–SRR34777150, SRR34777187–SRR34777190, SRR34777192–SRR34777201, SRR34777203–SRR34777212, SRR34777214, SRR34777247–SRR34777255, SRR34777257–SRR34777266, SRR34777268–SRR34777277, SRR34777279–SRR34777288, SRR34777290–SRR34777299, SRR34777301–SRR34777310), and the genome assembly generated in this study has been deposited in the NCBI under the accession number GCA_054095995.1, datasets used to generate the assembly are available under the accession number PRJNA1297316. Sanger sequences have been deposited in GenBank with accession numbers in Supplementary Data 1. Other genomes used in this study include *Hyalella azteca* (GCA_000764305.4)⁹⁴, *Parhyale hawaiiensis* (GCA_001587735.2)³⁷, *Hirondellea gigas* (CNGBdb Project ID CNP0005374)⁹⁵, *Trinorchestia longiramus* (GCA_006783055.1)⁹⁶, *Morinoia aosen* (GCA_030386875.1)⁷¹, *Floresorchestia mkomani* (SRR23898670 under PRJNA938803)⁷¹, *Cochinorchestia* sp. (SRR23898667 under PRJNA938803)⁷¹, *Platorchestia pacifica* (SRR23898669 under PRJNA938803)⁷¹. Four annual mean environmental variables (sea surface temperature, sea surface salinity, ocean current direction, and ocean current velocity) are from Bio-ORACLE (<https://www.bio-oracle.org/>), the variable “distance from shore” from the MARSPEC database (<http://marspec.weebly.com>). Sea surface ocean currents data from Global Ocean Ensemble Physics Reanalysis (GOEPR) are available in Copernicus Marine Environment Monitoring Service (CMEMS; <https://marine.copernicus.eu/>). The bathymetric data can be obtained from the ETOPO1 database (<https://www.ngdc.noaa.gov/mgg/global/relief/ETOPO1/>). Sampling data can be found in Supplementary Data 1. Results of genetic offsets are available in Supplementary Data 2–6, and gene family can be found in Supplementary Data 7. Source data are provided in this paper.

Code availability

Analysis scripts can be found at Figshare (<https://doi.org/10.6084/m9.figshare.29614727>)¹⁰⁰, and Code Ocean deposition (<https://doi.org/10.24433/CO.2066999.v1>).

References

- Carlton, J. et al. Tsunami-driven rafting: Transoceanic species dispersal and implications for marine biogeography. *Science* **357**, 1402–1406 (2017).
- Fraser, C. et al. Antarctica’s ecological isolation will be broken by storm-driven dispersal and warming. *Nat. Clim. Change* **8**, 704–708 (2018).
- Villarino, E. et al. Large-scale ocean connectivity and planktonic body size. *Nat. Commun.* **9**, 142 (2018).
- Gillespie, R. et al. Long-distance dispersal: a framework for hypothesis testing. *Trends Ecol. Evol.* **27**, 47–56 (2012).
- MacArthur, R. H. & Wilson, E. O. *The Theory of Island Biogeography* (Princeton Univ. Press, 1967)
- Fraser, C. I., Nikula, R. & Waters, J. M. Oceanic rafting by a coastal community. *Proc. Biol. Sci.* **278**, 649–655 (2010).
- Collins, C. J., Fraser, C. I., Ashcroft, A. & Waters, J. M. Asymmetric dispersal of southern bull-kelp (*Durvillaea antarctica*) adults in coastal New Zealand: testing an oceanographic hypothesis. *Mol. Evol.* **19**, 4572–4580 (2010).
- Waters, J. M. Seaweed rafts. *Curr. Biol.* **31**, R1510–R1511 (2021).
- Yu, L. et al. Ocean current patterns drive the worldwide colonization of eelgrass (*Zostera marina*). *Nat. Plants* **9**, 1207–1220 (2023).
- Kling, M. M. & Ackerly, D. D. Global wind patterns shape genetic differentiation, asymmetric gene flow, and genetic diversity in trees. *Proc. Natl. Acad. Sci. USA* **118**, e2017317118 (2021).
- Wilson, L. J. et al. Climate-driven changes to ocean circulation and their inferred impacts on marine dispersal patterns. *Glob. Ecol. Biogeogr.* **25**, 923–939 (2016).
- Peng, Q. et al. Surface warming-induced global acceleration of upper ocean currents. *Sci. Adv.* **8**, eabj8394 (2022).
- Röthig, T. et al. Sweet, Human-induced salinity changes impact marine organisms and ecosystems. *Global Change Biol.* **29**, 4731–4749 (2023).
- van der Stocken, T., Vanschoenwinkel, B., Carroll, D., Cavanaugh, K. C. & Koedam, N. Mangrove dispersal disrupted by projected changes in global seawater density. *Nat. Clim. Change* **12**, 685–691 (2022).
- Wildish, D. J. Evolutionary ecology of driftwood talitrids: a review. *Zoosyst. Evol.* **93**, 353–361 (2017).
- Fanini, L. & Lowry, J. Coastal talitrids and connectivity between beaches: A behavioural test. *J. Exp. Mar. Biol. Ecol.* **457**, 120–127 (2014).
- He, Z., Feng, M., Wang, D. & Slawinski, D. Contribution of the Karimata Strait transport to the Indonesian Throughflow as seen from a data assimilation model. *Cont. Shelf Res.* **92**, 16–22 (2015).
- Wang, Y. et al. Seasonal variation of water transport through the Karimata Strait. *Acta Oceanol. Sin.* **38**, 47–57 (2019).
- Sholihah, A. et al. Impact of Pleistocene eustatic fluctuations on evolutionary dynamics in Southeast Asian biodiversity hotspots. *Syst. Biol.* **70**, 940–960 (2021).
- Hernawan, U. E. et al. Historical processes and contemporary ocean currents drive genetic structure in the seagrass *Thalassia hemprichii* in the Indo-Australian Archipelago. *Mol. Ecol.* **26**, 1008–1021 (2017).
- Hou, Z. & Li, S. Intraspecific or interspecific variation: delimitation of species boundaries within the genus *Gammarus* (Crustacea, Amphipoda, Gammaridae), with description of four new species: delimitation of *Gammarus* species boundaries. *Zool. J. Linn. Soc. Lond.* **160**, 215–253 (2010).
- Li, H. & Durbin, R. Inference of human population history from individual whole-genome sequences. *Nature* **475**, 493–496 (2011).
- Gronau, I., Hubisz, M. J., Gulko, B., Danko, C. G. & Siepel, A. Bayesian inference of ancient human demography from individual genome sequences. *Nat. Genet.* **43**, 1031–1034 (2011).
- Pickrell, J. K. & Pritchard, J. K. Inference of population splits and mixtures from genome-wide allele frequency data. *PLoS Genet.* **8**, e1002967 (2012).
- Excoffier, L., Dupanloup, I., Huerta-Sánchez, E., Sousa, V. C. & Foll, M. Robust demographic inference from genomic and SNP data. *PLoS Genet.* **9**, e1003905 (2013).
- Hodel, R. G. et al. Terrestrial species adapted to sea dispersal: differences in propagule dispersal of two Caribbean mangroves. *Mol. Ecol.* **27**, 4612–4626 (2018).
- Bennett, A. *Lagrangian Fluid Dynamics*. (Cambridge University, Cambridge, 2006).

28. Dagestad, R. Öhrs, K. F., Breivik, J. & Ådlandsvik, Ø B. OpenDrift v1.0: a generic framework for trajectory modelling. *Geosci. Model Dev.* **11**, 1405–1420 (2018).
29. Gougherty, A. V., Keller, S. R. & Fitzpatrick, M. C. Maladaptation, migration and extirpation fuel climate change risk in a forest tree species. *Nat. Clim. Change* **11**, 166–171 (2021).
30. Ellis, N., Smith, S. J. & Pitcher, C. R. Gradient forests: Calculating importance gradients on physical predictors. *Ecology* **93**, 156–168 (2012).
31. Chiu, C. I. et al. Termite salinity tolerance and potential for transoceanic dispersal through rafting. *Ecol. Entomol.* **46**, 106–116 (2021).
32. Jaspers, C. et al. Invasion genomics uncover contrasting scenarios of genetic diversity in a widespread marine invader. *Proc. Natl. Acad. Sci. USA* **118**, e2116211118 (2021).
33. Fritchot, E., Schoville, S., Bouchard, D. & François, G. O. Testing for associations between loci and environmental gradients using latent factor mixed models. *Mol. Biol. Evol.* **30**, 1687–1699 (2013).
34. Forester, B. R., Jones, M., Joost, R. S., Landguth, E. L. & Lasky, J. R. Detecting spatial genetic signatures of local adaptation in heterogeneous landscapes. *Mol. Ecol.* **25**, 104–120 (2016).
35. Asaduzzaman, M. et al. Morpho-genetic divergence and adaptation of anadromous Hilsa shad (*Tenualosa ilisha*) along their heterogeneous migratory habitats. *Front. Mar. Sci.* **7**, <https://doi.org/10.3389/fmars.2020.00554> (2020).
36. Jombart, T., Devillard, S. & Balloux, F. Discriminant analysis of principal components: A new method for the analysis of genetically structured populations. *BMC Genet.* **11**, 94 (2010).
37. Kao, D. et al. The genome of the crustacean *Parhyale hawaiiensis*, a model for animal development, regeneration, immunity and lignocellulose digestion. *Elife* **5**, e20062 (2016).
38. Cantarel, B. L. et al. The Carbohydrate-Active EnZymes database (CAZy): an expert resource for glycogenomics. *Nucleic Acids Res.* **37**, D233–D238 (2009).
39. Petrick, B. et al. Glacial Indonesian Throughflow weakening across the mid-Pleistocene climatic transition. *Sci. Rep.* **9**, 16995 (2019).
40. Zheng, B., Xu, Q. & Shen, Y. The relationship between climate change and Quaternary glacial cycles on the Qinghai–Tibetan Plateau: review and speculation. *Quatern. Int.* **97**, 93–101 (2002).
41. van der Zee, J. P. et al. Demographic changes in Pleistocene sea turtles were driven by past sea level fluctuations affecting feeding habitat availability. *Mol. Ecol.* **31**, 1044–1056 (2022).
42. Holt, B. G. et al. An update of Wallace’s zoogeographic regions of the world. *Science* **339**, 74–78 (2013).
43. Skeels, A. et al. Paleoenvironments shaped the exchange of terrestrial vertebrates across Wallace’s Line. *Science* **381**, 86–92 (2023).
44. Barber, P. H., Palumbi, S. R., Erdmann, M. V. & Moosa, M. K. A. marine Wallace’s line?. *Nature* **406**, 692–693 (2000).
45. Fraser, C. I. et al. Southern Hemisphere coasts are biologically connected by frequent, long-distance rafting events. *Curr. Biol.* **32**, 3154–3160 (2022).
46. Liu, J., Lindstrom, A. J., Chen, Y., Nathan, R. & Gong, X. Congruence between ocean-dispersal modelling and phylogeography explains recent evolutionary history of *Cycas* species with buoyant seeds. *New Phytol.* **232**, 1863–1875 (2021).
47. Murphy, E., Nistor, I., Cornett, A., Wilson, J. & Pilechi, A. Fate and transport of coastal driftwood: A critical review. *Mar. Pollut. Bull.* **170**, 112649 (2021).
48. Layton, K. K. S. et al. Predicting the future of our oceans—Evaluating genomic forecasting approaches in marine species. *Global Change Biol.* **30**, e17236 (2024).
49. Chen, Y. et al. Incorporating adaptive genomic variation into predictive models for invasion risk assessment. *Environ. Sci. Eco-tech.* **18**, 100299 (2024).
50. Bay, R. A. et al. Genomic signals of selection predict climate driven population declines in a migratory bird. *Science* **359**, 83–86 (2018).
51. Ferrer Obiol, J. et al. Evolutionarily distinct lineages of a migratory bird of prey show divergent responses to climate change. *Nat. Commun.* **16**, 3503 (2025).
52. Layton, K. K. S. et al. Genomic evidence of past and future climate-linked loss in a migratory Arctic fish. *Nat. Clim. Change* **11**, 158–165 (2021).
53. Lotterhos, K. E. Interpretation issues with “genomic vulnerability” arise from conceptual issues in local adaptation and maladaptation. *Evol. Lett.* **8**, 331–339 (2024).
54. Aguirre-Liguori, J. A., Ramirez-Barahona, S. & Gaut, B. S. The evolutionary genomics of species’ responses to climate change. *Nat. Ecol. Evol.* **5**, 1350–1360 (2021).
55. Barrett, N. J. et al. Molecular responses to thermal and osmotic stress in Arctic intertidal mussels (*Mytilus edulis*): the limits of resilience. *Genes* **13**, 155 (2022).
56. Rumberger, C. et al. Selection Over Small and Large Spatial Scales in the Face of High Gene Flow. *Mol. Ecol.* **34**, e17700 (2025).
57. Gleason, L. U. & Burton, R. S. Phenotypic evidence for local adaptation to heat stress in the marine snail *Chlorostoma* (formerly *Tegula*) *funnebralis*. *J. Exp. Mar. Biol. Ecol.* **448**, 360–366 (2013).
58. Nuñez, J. C. B. et al. From Tides to Nucleotides: Genomic Signatures of Adaptation to Environmental Heterogeneity in Barnacles. *Mol. Ecol.* **30**, 6417–6433 (2021).
59. Lee, C. E. Ion transporter gene families as physiological targets of natural selection during salinity transitions in a copepod. *Physiology* **36**, 335–349 (2021).
60. Hastings, R. A. et al. Climate change drives poleward increases and equatorward declines in marine species. *Curr. Biol.* **30**, 1572–1577 (2020).
61. Hoffmann, A. A., Weeks, A. R. & Sgrò, C. M. Opportunities and challenges in assessing climate change vulnerability through genomics. *Cell* **184**, 1420–1425 (2021).
62. Rellstab, C., Dauphin, B. & Exposito-Alonso, M. Prospects and limitations of genomic offset in conservation management. *Evol. Appl.* **14**, 1202–1212 (2021).
63. Stern, D. & Lee, C. Evolutionary origins of genomic adaptations in an invasive copepod. *Nat. Ecol. Evol.* **4**, 1084–1094 (2020).
64. Liu, H., Wang, X., Liu, Z., Li, S. & Hou, Z. Osmoregulatory evolution of gills promoted salinity adaptation following the sea–land transition of crustaceans. *Mar. Life Sci. Technol.* **7**, 205–217 (2025).
65. Cui, Z. et al. The Chinese mitten crab genome provides insights into adaptive plasticity and developmental regulation. *Nat. Commun.* **12**, 2395 (2021).
66. Whitehead, A., Roach, J. L., Zhang, S. & Galvez, F. Genomic mechanisms of evolved physiological plasticity in killifish distributed along an environmental salinity gradient. *Proc. Natl. Acad. Sci. USA* **108**, 6193–6198 (2011).
67. Ghalambor, C. K., McKay, J. K., Carroll, S. P. & Reznick, D. N. Adaptive versus non-adaptive phenotypic plasticity and the potential for contemporary adaptation in new environments. *Funct. Ecol.* **21**, 394–407 (2007).
68. Thiel, M. Rafting of benthic macrofauna: important factors determining the temporal succession of the assemblage on detached macroalgae. *Hydrobiologia* **503**, 49–57 (2003).
69. Gibson, R. N. & Robb, L. Piscine predation on juvenile fishes on a Scottish sandy beach. *J. Fish Biol.* **49**, 120–138 (1996).
70. King, A. J. et al. Molecular insight into lignocellulose digestion by a marine isopod in the absence of gut microbes. *Proc. Natl. Acad. Sci. USA* **107**, 5345–5350 (2010).

71. Liu, H. et al. Marine-montane transitions coupled with gill and genetic convergence in extant crustacean. *Sci. Adv.* **9**, eadg4011 (2023).
72. Bolger, A. M., Lohse, M. & Usadel, B. Trimmomatic: a flexible trimmer for Illumina sequence data. *Bioinformatics* **30**, 2114–2120 (2014).
73. Alonge, M. et al. Automated assembly scaffolding using RagTag elevates a new tomato system for high-throughput genome editing. *Genome Biol.* **23**, 258 (2022).
74. Li, H. & Durbin, R. Fast and accurate short read alignment with Burrows–Wheeler transform. *Bioinformatics* **25**, 1754–1760 (2009).
75. McKenna, A. et al. The Genome Analysis Toolkit: a MapReduce framework for analyzing next-generation DNA sequencing data. *Genome Res.* **20**, 1297–1303 (2010).
76. Danecek, P. et al. The variant call format and VCFtools. *Bioinformatics* **27**, 2156–2158 (2011).
77. Danecek, P. et al. Twelve years of SAMtools and BCFtools. *Giga-science* **10**, gjab008 (2021).
78. Purcell, S. et al. PLINK: a tool set for whole-genome association and population-based linkage analyses. *Am. J. Hum. Genet.* **81**, 559–575 (2007).
79. Papa, Y., Morrison, M. A., Wellenreuther, M. & Ritchie, P. A. Genomic stock structure of the marine teleost tarakihi (*Nemadactylus macropterus*) provides evidence of potential fine-scale adaptation and a temperature-associated cline amid panmixia. *Front. Ecol. Evol.* **10**, 862930 (2022).
80. Stamatakis, A. RAxML version 8: a tool for phylogenetic analysis and post-analysis of large phylogenies. *Bioinformatics* **30**, 1312–1313 (2014).
81. Zheng, X. SNPRelate: parallel computing toolset for genome-wide association studies. *R Package Version* **95**, B9 (2012).
82. Alexander, D. H., Novembre, J. & Lange, K. Fast model-based estimation of ancestry in unrelated individuals. *Genome Res.* **19**, 1655–1664 (2009).
83. Malinsky, M., Matschiner & Svardal, M. H. Dsuite-fast *D*-statistics and related admixture evidence from VCF files. *Mol. Ecol. Resour.* **21**, 584–595 (2021).
84. Pante, E. & Simon-Bouhet, B. marmap: a package for importing, plotting and analyzing bathymetric and topographic data in R. *PLoS ONE* **8**, e73051 (2013).
85. Amante, C. & Eakins, B. W. *ETOPO11 Arc-Minute Global Relief Model: Procedures, Data Sources and Analysis*. NOAA Technical Memorandum NESDIS NGDC-24 (NOAA, 2009).
86. Sbrocco, E. J. & Barber, P. H. MARSPEC: ocean climate layers for marine spatial ecology: Ecological Archives E094–086. *Ecology* **94**, 979 (2013).
87. Frichot, E. & François, O. LEA: an R package for landscape and ecological association studies. *Methods Ecol. Evol.* **6**, 925–929 (2015).
88. Capblancq, T. & Forester, B. R. Redundancy analysis: a Swiss Army Knife for landscape genomics. *Methods Ecol. Evol.* **12**, 2298–2309 (2021).
89. Xie, C. et al. KOBAS 2.0: a web server for annotation and identification of enriched pathways and diseases. *Nucleic Acids Res.* **39**, W316–W322 (2011).
90. Li, B. & Dewey, C. N. RSEM: Accurate transcript quantification from RNA-Seq data with or without a reference genome. *BMC Bioinform.* **12**, 323 (2011).
91. Love, M., Huber, W. & Anders, S. Moderated estimation of fold change and dispersion for RNA-seq data with DESeq2. *Genome Biol.* **15**, 1–21 (2014).
92. Jombart, T. *adegenet*: A R package for the multivariate analysis of genetic markers. *Bioinformatics* **24**, 1403–1405 (2008).
93. Yin, Y. et al. dbCAN: a web resource for automated carbohydrate-active enzyme annotation. *Nucleic Acids Res.* **40**, W445–W451 (2012).
94. Poynton, H. C. et al. The Toxicogenome of *Hyalella azteca*: A Model for Sediment Ecotoxicology and Evolutionary Toxicology. *Environ. Sci. Technol.* **52**, 6009–6022 (2018).
95. Zhang, H. et al. The amphipod genome reveals population dynamics and adaptations to hadal environment. *Cell* **188**, 1378–1392 (2025).
96. Patra, A. K. et al. First draft genome for the sand-hopper *Trinorchestia longiramus*. *Sci. Data* **7**, 85 (2020).
97. Mistry, J., Finn, R. D., Eddy, S. R., Bateman, A. & Punta, M. Challenges in homology search: HMMER3 and convergent evolution of coiled-coil regions. *Nucleic Acids Res.* **41**, e121–e121 (2013).
98. Emms, D. M. & Kelly, S. OrthoFinder: phylogenetic orthology inference for comparative genomics. *Genome Biol.* **20**, 238 (2019).
99. De Bie, T., Cristianini, N., Demuth, J. P. & Hahn, M. W. CAFE: a computational tool for the study of gene family evolution. *Bioinformatics* **22**, 1269–1271 (2006).
100. Liu, H. et al. Code and data for ‘Genomics of rafting crustaceans reveals adaptation to climate change in tropical oceans’. Figshare <https://doi.org/10.6084/m9.figshare.29614727> (2025).

Acknowledgements

We thank Baocheng Guo, Yilin Chen, Dezhi Zhang, Bingyue Zhu, Tongyao Jiang, Zhe Zhao, Fengyuan Li, and Pengyu Jin for helpful discussion; Zeyu Liu and Wenpei Xin for help in salinity experiments; Knut-Frode Dagestad for help in OpenDrift analysis; Zilong Bai and O. Alfaruq for assistance in field collection. This study was supported by the National Natural Science Foundation of China (grant number 32470474 for Z.H., 32500387 for H.L.), the International Partnership Program of the Chinese Academy of Sciences (grant number 073GJHZ2024043MI for Z.H. and H.L.), the Institute of Zoology, Chinese Academy of Sciences (2023IOZ0104 and 2024IOZ0108 for Z.H.), Beijing Natural Science Foundation (grant number 5244045 for H.L.).

Author contributions

H.L. and Z.H. designed research; H.L., M.H., and Z.W. performed research; W.J.C. and S.L. collected samples and participated in discussions; H.L. and Z.H. wrote the manuscript; J.M.W. reviewed and edited the manuscript. All authors proofread and approved the manuscript.

Competing interests

The authors declare no competing interests.

Additional information

Supplementary information The online version contains supplementary material available at <https://doi.org/10.1038/s41467-026-69173-x>.

Correspondence and requests for materials should be addressed to Zhonghe Hou.

Peer review information *Nature Communications* thanks Jilian Xiong, Zhiqiang Ye and the other anonymous reviewer(s) for their contribution to the peer review of this work. A peer review file is available.”

Reprints and permissions information is available at <http://www.nature.com/reprints>

Publisher’s note Springer Nature remains neutral with regard to jurisdictional claims in published maps and institutional affiliations.

Open Access This article is licensed under a Creative Commons Attribution-NonCommercial-NoDerivatives 4.0 International License, which permits any non-commercial use, sharing, distribution and reproduction in any medium or format, as long as you give appropriate credit to the original author(s) and the source, provide a link to the Creative Commons licence, and indicate if you modified the licensed material. You do not have permission under this licence to share adapted material derived from this article or parts of it. The images or other third party material in this article are included in the article's Creative Commons licence, unless indicated otherwise in a credit line to the material. If material is not included in the article's Creative Commons licence and your intended use is not permitted by statutory regulation or exceeds the permitted use, you will need to obtain permission directly from the copyright holder. To view a copy of this licence, visit <http://creativecommons.org/licenses/by-nc-nd/4.0/>.

© The Author(s) 2026